Journal of Energy Storage 54 (2022) 105217

Contents lists available at ScienceDirect

Journal of Energy Storage

journal homepage: www.elsevier.com/locate/est

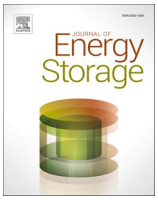

Research Papers

Thermal evaluation of lithium-ion batteries: Defining the cylindrical cell cooling coefficient

M. Waseem Marzook [a], Alastair Hales [a,b,*], Yatish Patel [a], Gregory Offer [a], Monica Marinescu [a]

[a] Imperial College London, Mechanical Engineering Department, UK
[b] University of Bristol, Department of Mechanical Engineering, UK

ARTICLE INFO

Keywords:
Battery heat generation
Battery thermal management
Cell cooling coefficient
Lithium-ion battery
Cylindrical lithium-ion cell
Cylindrical base cooling

ABSTRACT

Managing temperatures of lithium-ion cells in battery packs is crucial to ensuring their safe operation. However, thermal information provided on typical cell datasheets is insufficient to identify which cells can be easily thermally managed. The Cell Cooling Coefficient (CCC) aims to fill this gap, as a metric that defines the thermal dissipation from a cell when rejecting its own heat. While the CCC has been defined and used for pouch cells, no similar measure has been proven for cylindrical cells. This work successfully defines and measures the CCC for cylindrical cells under base cooling (CCC_{Base}), defined as the heat rejected through the base divided by the temperature difference from the base to positive cap. Using a non-standard, electrically optimised connection, the maxima for CCC_{Base} of an LG M50T (21700) and Samsung 30Q (18650) cell are successfully measured to be 0.139 and 0.115 W K^{-1}, respectively. Even though the 21700 has a higher CCC_{Base}, indicating that the cell can be cooled more efficiently, comparing the CCC_{Base} per area the 18650 can reject 13 % more heat for a given cooled area. A worked example demonstrates the equal importance of understanding heat generation alongside the CCC, for both cell design and down selecting cells.

1. Introduction

Lithium-ion batteries are ubiquitous, from mobile phones to electric vehicles (EVs), with the ability to fast charge and have a long cycle life being two of the most sought-after cell attributes. Both of these attributes are strongly influenced by the management of heat in a battery pack; cell temperatures must be controlled in an effective manner in order to limit degradation [1] and prevent overheating and thermal runaway [2]. In order to control temperature and design effective and efficient thermal management systems for battery packs, the thermal properties of cells must be quantified and understood.

However, standard thermal properties, such as thermal conductivity, conductance, diffusivity and the Biot number, are not appropriate measures for lithium-ion cells. The main difference is that battery cells are power and heat sources rather than passive elements [3]. Moreover, these standard thermal properties are not easily measurable in a meaningful way, as the internal geometry and composition of a cell are complex and inhomogeneous, such that bulk measurements can be misleading if the anisotropic behaviour is not modelled accurately [4,21]. The thermal properties of each component material can be in principle measured [5], but evaporation of the electrolyte renders some measurements difficult and/or inaccurate [6]. Even if measurements for each component material could be taken accurately, measuring the thermal properties of all internal interfaces between the various layers is very difficult and ignoring them leads to inaccuracy when modelling cell thermal behaviour [7].

The cell cooling coefficient (CCC) is a thermal metric designed to describe the application-relevant thermal properties of lithium-ion cells, defining the amount of self-generated heat a cell can reject through a cooled surface, for a given temperature difference across its body. As a result, the CCC is measured in Watts per Kelvin (W K^{-1}) [8]. This definition describes the heat rejection capability of a cell's surface, allowing for the comparison of geometrically different cells. The CCC is specific to each surface of a cell, thus each cell is characterised by multiple CCC values, one for each potential cooling approach. For pouch cells, CCC_{tabs} and CCC_{surf} have been measured for tab [8] and surface [9] cooling, respectively, allowing a comparison of the effectiveness of the two cooling methods. The CCC can also be used as an optimisation target, as it can serve as a measure of improvements in the thermal performance of cells through better cell design [10]. The concept and implementation of

* Corresponding author at: University of Bristol, Department of Mechanical Engineering, UK.
E-mail address: a.hales@bristol.ac.uk (A. Hales).

https://doi.org/10.1016/j.est.2022.105217
Received 21 April 2022; Received in revised form 13 June 2022; Accepted 24 June 2022
Available online 9 July 2022

measuring the CCC for cylindrical lithium-ion cells is yet to be addressed and forms the purpose of this work.

Cylindrical cells are a popular form of lithium-ion battery used in a wide range of applications, from handheld appliances (i.e., power tools) to EVs (Tesla). In these cells the electrode stack is rolled into a spiral and inserted into a cylindrical can. Tabs from the negative current collector are welded on the inside of the base of the can and tabs from the positive current collector are welded to a positive cap. The positive cap usually contains several safety devices, such as the Positive Thermal Coefficient (PTC) [11], a Current Interrupt Device (CID) and a safety vent [12]. These devices are designed to protect and prevent the cell from failing and reaching thermal runaway, however they are not effective in all failure circumstances: PTC devices were shown to fail when in series strings above eight [13], and safety vents were shown to not vent reliably when releasing pressure built up inside the can of the cell [12]. These devices are included to help reduce consequence should the cell's overheat in operation, but they are not designed to reduce the likelihood of such an event occurring. For this, we use thermal management systems – active cooling applied in various forms to maintain an ideal operating temperature for the cell, well below the temperature at which the CID, PTC or vent must come into use.

The various features of cylindrical cells, including the spiral electrode stack, welded tabs and safety devices, result in complex thermal pathways and heat generation profiles within these cells. The relatively high resistance of the positive safety cap in cylindrical cells leads to highly concentrated, localised heat generation at one end of the cell [14]. Defining and measuring the CCC for these cells can predict and help interpret their thermal performance, including the effect of the complex heat generation profile.

The three most common thermal management strategies for cylindrical cell packs are dual terminal, surface/can [15] and base cooling [16]. Terminal cooling denotes the case in which both ends of the cell are cooled, on the electrical terminals. This can be done using a cooling fluid, via direct contact with the cell, or indirect contact through a cooling plate or fin. Can cooling defines cooling the side of the cell can, where the proportion of surface cooled is variable between different applications. This method usually reduces the packing factor, as the cells need to be spaced further apart, in order to allow the cooling medium or the cooling fins to be inserted in-between the cells [15]. Base cooling involves cooling the negative end of all cells on a flat cooling plate. Base cooling is widely popular, as it offers the simplest thermal system design, but it adds challenges to the electrical design, as connections can no longer be made to the base of the cell. Instead, both electric connections need to be made at the top of the cell, where both the positive and negative terminals are available. Importantly, base cooling is expected to cause the highest temperature gradients axially within the cell, when compared to the other two cooling strategies [17].

This study focuses on establishing the first method for measuring a meaningful CCC for cylindrical cells, to help aid the comparison of the thermal dissipation capability of different cylindrical cells. Firstly, an improved representation of the CCC for any cell is formulated, to aid in its calculation. A meaningful CCC can only be obtained if it covers a range of operating conditions that is reflective of the intended application, and its value can be measured consistently within ±10 % measurement error. This uncertainty value has been chosen based on thermal standards observed by the National Physics Laboratory, where uncertainties of up to ±6.1 % are used for reference material specimens [18]. These reference materials are manufactured from highly consistent, homogeneous substances – the ideal case for thermal metrology. A cell, which has a complex composite structure and anisotropic thermal properties, presents a more challenging test case, thus uncertainties are expected to be higher, and ±10 % has been chosen. The cooling method of choice for this CCC work is base cooling of cylindrical cells. This will be measured using a specifically designed rig for the comparison of two typical cell sizes, 18650 and 21700. The measurement of CCC values for these two popular cell sizes can be adopted for the numerous cells available on the market, allowing end users to compare cells thermally prior to any testing, saving countless test hours that would otherwise be needed to characterise the cells electrothermally.

2. Theory

The CCC is defined by, the amount of internal heat rejected from a cell's cooled surface(s) ($\dot{Q}$), divided by the temperature difference from the cell's cooled surface(s) to the hottest point of the cell (ΔT), in steady state, as shown in Eq. (1).

$$CCC = \dot{Q} \Big/ \Delta T \tag{1}$$

The CCC is a cell-level thermal metric and can be thought of as a material property for a cell. It should be noted that the CCC is a different characteristic from the heat transfer coefficient, which defines the heat transfer between a cooling medium and surface. It can more closely be compared to an effective thermal resistance for a body (cell), defining the ratio of heat flow to thermal difference. However, instead of external heat passing through the body, the CCC describes a system where heat is generated within the body and fully rejected from a specified surface(s). The anisotropic nature of thermal conductivity, diffusivity, and heat generation in a cell result in the CCC being defined separately for each combination of surfaces that are cooled (dual-tab, single tab, dual-surface, single surface, base, etc.). There are four published articles on the topic, identifying, defining and measuring CCC values for different types of cells and surfaces of cooling. These works cover dual-tab [8] and single surface [9,10] cooling of pouch cells, as well as single-sided surface cooling for prismatic cells [19].

The CCC measurement method involves constant current pulsing a cell at 1 Hz in a setup with controlled thermal boundary conditions where the temperature is measured at various positions around the cell. Once the cell reaches steady state thermal conditions the value of CCC is calculated through the measured heat rejection and temperature difference as per Eq. (1). This test is done at multiple current magnitudes and cooling temperatures, with the calculated CCC values plotted on a graph of CCC against heat generation (assumed to be equal to heat rejection), as shown in Fig. 1. In these works, the plot of CCC versus measured heat generation is used to quantify the correlation between the two variables, where a horizontal line is associated with no correlation. A dependency of the CCC on the measured heat generation, i.e. a non-horizontal plot, is assumed to indicate a correlation between the two, which, in turn, is assumed to be caused by limitations in the experimental procedure, such as difficulties in managing heat loss, accurately measuring heat flow, and measuring accurate cell thermal differences. The test rig designed to determine CCC_{tab} was found to lead to no observable correlation [8], while the first proposed method to determine CCC_{surf} was found to lead to correlations, due to the non-zero slopes of the lines in Fig. 1 [9]. The correlation in these results was described to be due to heat losses in the experimental rig, thus to eliminate this from the determined value, the CCC was extrapolated back to zero heat generation, Q = 0 W, where heat losses are zero. A more complex test rig for CCC_{surf} allowed for improved thermal control over the cell, thus eliminating the apparent correlation between CCC and heat generation [10]. Both of these solutions result in a CCC derivation process that is more complicated than was originally intended.

According to Eq. (1) the CCC is the slope on a Q vs. ΔT plot. If the CCC of a given cell is constant, then all experimentally measured heat generation values should lie on a single line on a plot vs. ΔT, and the CCC value for the considered cooling scheme is the gradient of the linear fit of $Q = f(\Delta T)$. Fig. 2 re-illustrates the pouch cell data shown in Fig. 1 [9], together with the results from the other two publications on CCC [8,10], in the alternative way proposed above.

For zero measured temperature gradient there is no heat flow through the cell, indicating that {0,0} is a point that must lie on the

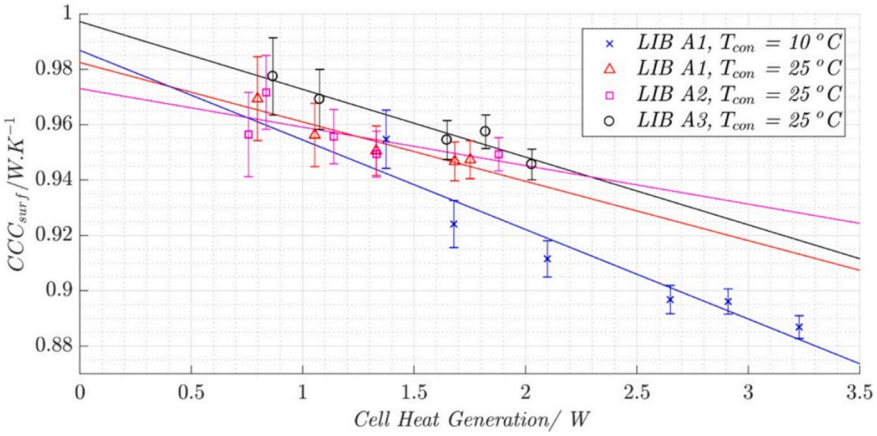

Fig. 1. CCC_{surf} vs. measured heat generation for a 5 Ah Kokam pouch cell for cooling on one surface at temperature Tcon. LIB A1-3 represent data from the three 5 Ah Kokam cells tested under identical conditions.
Reproduced with permission from [[9]].

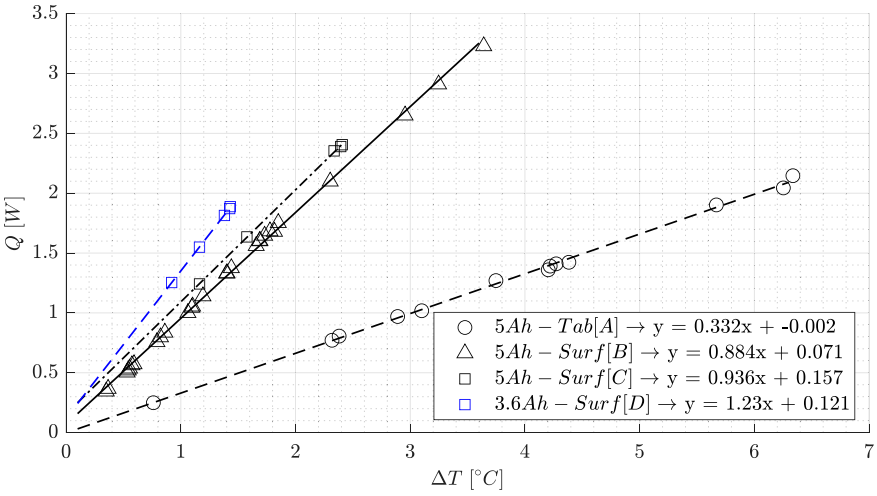

Fig. 2. Previously presented CCC data displayed on a plot with different axes: Q vs. ΔT. Data obtained from the following references: A. [8], B. [9], C & D. [10].

linear fit. However, two of the lines that best fit the data have, in fact, significant non-zero Y-intercepts. This is likely caused by the limited temperature range for which these results were obtained, leading to a significant extrapolation from the dataset down to zero. This error results in an important new criterion for accurate CCC measurement: experimental data must cover a sufficient thermal range for the cell and cooling system, this means the data should start at low temperature differences and have a range of points leading up to the maximum realistic ΔT that keeps the cell within safe operation for the cooling system, both electrically and thermally.

3. Base cooling experimental setup

The CCC for base cooling of cylindrical cells (CCC_{Base}) is approximated as the heat rejected from the base of the cell divided by the measured temperature difference between the top and base of the cell. The CCC_{Base} is determined for two cells of different sizes. Firstly, an LG INR21700 M50T cell is considered, a high energy cell with a silicon doped graphite anode and an NMC811 cathode and a nominal capacity of 5 Ah. Secondly, a Samsung INR18650 30Q cell is evaluated, considered a mixed power and energy cell, with a silicon doped graphite anode and an NCA cathode and a nominal capacity of 3 Ah.

3.1. Cell connection

A typical base cooled cylindrical cell has its external negative electrical connection at the top shoulder of the cell instead of at the base of the cell, to avoid hindering the cooling path. This choice of connection allows all cells to be oriented in the same direction in a pack. Connecting to the shoulder of a cylindrical cell requires sophisticated and expensive welding techniques, such as laser or ultrasonic welding, due to the relatively small surface area available for contact. This type of connection cannot be done cheaply or quickly, even for a single cell. These types of welding equipment can be expensive to purchase or use; and will require the design and manufacture of custom rigs to hold the cell and connections in place for welding. In this work, a more traditional tab connection is used instead, at the base of the cell, allowing for an easier measurement of CCC_{Base}. A tab is spot welded as closely to the edge of the base as possible in order to minimise its effect on the cooling path. This connection is expected to yield the theoretical maximum for the CCC measurement for base cooling because the heat generation of the negative connection is as close as possible to the heat sink, allowing for the shortest heat conduction path out of the cell. Moving the connection up to the top of the cell would shift this heat to the furthest point away from cooling, increasing the temperature gradient in the cell, whilst marginally increasing heat generation, thus lowering the CCC.

3.2. CCC rig design

A schematic of the rig is illustrated in Fig. 3. As is the case for the previous CCC measurement rigs [8–10], the experimental rig is designed to restrict all thermal pathways except for the one of interest, attempting to create adiabatic boundary conditions on all surfaces not being actively cooled. The cooling path, in this case the brass rod, is designed to develop a significant measurable temperature gradient along its length when heat flows from the cell. This rig is additionally designed to measure the axial heat losses from the cell, via the placement of an additional thermocouple (TC), denoted as number 11 in Fig. 3, in the insulation below the positive end of the cell, which is expected to be the hottest point on the cell, as well as additional TCs positioned along the Ni tabs connecting the cell (numbers 8, 9 and 10 in Fig. 3). Real images of the experimental rig can be found in supplementary material in Fig. 8.

The cooling fin comprises two aluminium plates, denoted as 'Top' and 'Base' in Fig. 3, that are bonded to a brass rod of dimensions 6 mm in diameter and 100 mm in length. The heat flow along the cooling fin is measured through two TCs, number 6 and 7, positioned 60 mm apart. A 40 × 40 mm Peltier element in contact with the aluminium top plate maintains the temperature of the plate using PID control to keep the temperature of the aluminium top plate constant. The electrical connection uses 8 mm × 0.15 mm (width × thickness) Ni tabs, spot welded using a Sunkko 709AD+ resistance welder. The negative Ni tab is positioned and welded at the edge of the base so that it minimises the obstruction to the cooling path. The Ni tabs are clamped between two brass blocks. Two ring terminated leads, one carrying current and the other one sensing voltage, are secured to each set of brass blocks in order to make a connection with the battery cycler, a Bio-Logic BCS-815.

All but one of the TCs used are k-type and are secured to the cell with MG Chemicals thermal epoxy (thermal conductivity – 1.22 W m K^{-1}). TC number 5 is a flat leaf k-type thermocouple, 0.1 mm in thickness, sandwiched between two layers of TGlobal thermal interface material (thermal conductivity - 12 W m K^{-1}), each 0.5 mm thick. This arrangement helps minimise the effect of this TC on the cooling path via the fin. A 4.9 N weight is placed on top of the fin, resulting in a pressure of 14 kPa at the base of the cell. The weighted fin applies pressure vertically on the set-up, ensuring good thermal contact between the fin and the base of the cell.

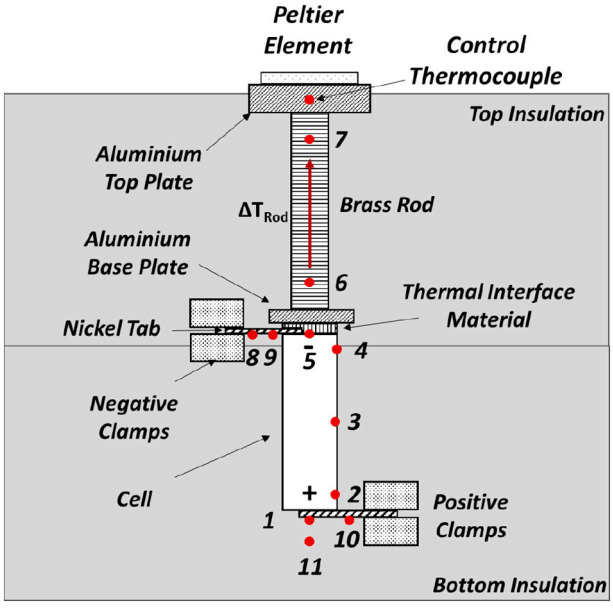

Fig. 3. Schematic of the CCC base cooling rig. All non-cooled surfaces are surrounded by insulation to create an adiabatic boundary condition. The base is cooled via a cooling fin designed to be thermally restrictive enough to generate a measurable thermal gradient when heat flows through it. A 4.9 N weight sits on top of the cooling fin to keep it secured to cell. This rig includes the measurement of axial losses at both ends of the cell (via numbers 8, 9, 10 & 11). The red dots denote placement of thermocouples. Not to scale. (For interpretation of the references to colour in this figure legend, the reader is referred to the web version of this article.)

For the calculation of CCC, the temperature difference is taken as that between TC 1 and 5. TC 2, 3 and 4 are positioned 10, 35 and 60 mm along the length of the cell, respectively, to monitor the temperature profile along the surface. This rig has three axial loss paths, two through the positive end and one through the negative. Losses through the insulation at the positive end are measured through TCs 1 and 11, which are 10 mm apart. Losses through the Ni tabs are measured through TC 1 and 10, and TC 8 and 9, which are 14 and 8 mm apart, respectively.

The 18650 cell is tested using the same experimental rig, with some slight changes. The axial loss TCs are removed, as they were already measured to be sufficiently low enough when the 21700 was tested. Additionally, TCs 2, 3 and 4 are positioned 10, 30 and 50 mm along the length of the cell, respectively (distances measured from the base of the cell).

3.3. Standard CCC procedure

The cell is charged and discharged via square wave current pulses, causing it to generate heat. During pulsing, the mean current is 0A, to prevent any net change in State of Charge (SOC). Current pulsing at 1 Hz is performed for 6 h to allow the cell and experimental rig to thermalise. Once the cell reaches thermal steady state, it generates a relatively constant amount of heat throughout the experiment. The experimental rig is kept in a Binder KB400 thermal chamber at constant ambient temperature. The set point temperature for the Peltier element is the same as the value set for the thermal chamber; it is controlled using a PID controller in order to maintain a constant temperature, despite the cell generating heat. Six pulsing experiments of increasing current amplitudes are performed, with a 90-minute rest after each set of pulses at a constant current amplitude. These six pulsing sets are designed to generate a sufficient range of temperature gradients across the cell to allow for a sufficient spread in the Q vs. ΔT plot, and thus a good baseline for a linear fit when calculating CCC. Each set of pulses are performed at a set operating point, where the operating point is defined by a predetermined combination of SOC and ambient temperature values. Table 1 shows the combinations of current, SOC and ambient cooling temperatures used for testing the LG M50T. The current amplitudes are selected such that they ensure that the dataset for each operating point includes a sufficient range of thermal differences for the cell, so that it can be used to find a reliable CCC for the specific operating point. Alternatively, all the data from multiple operating points can be combined to find an overall CCC for a cell.

Table 1
Combinations of experimental conditions tested for both LG M50T cells. For 50 % SOC all combinations were tested. For 25 % and 75 % SOC only the blue highlighted combinations were tested.

I (A) \ T (°C)	10	20	30
3.75			
5			
6.25			
7.5			
8.75			
10			

4. Results & discussion

4.1. 21700 testing

4.1.1. Current, temperature & SOC variation

To obtain a CCC with high confidence, it is important that the measured temperature gradient on the cell is large enough (>0.5 °C). The smallest temperature gradient is seen at the lowest current amplitude with the highest ambient temperature. At the opposite extreme, the highest current amplitude was chosen such that the cell temperature does not evolve above the safe operating temperature, even when operating at the highest ambient temperature. The maximum operating temperature allowed for these tests is 60 °C.

Fig. 4 shows the results of 18 pulsing sets, corresponding to all the combinations shown in Table 1, covering six currents at three cooling temperatures all performed at 50 % SOC. Additionally, it shows 8 pulsing sets, corresponding to the 4 combinations shown in blue in Table 1, performed at 25 % and 75 % SOC. The line of best fit has a negligible y-intercept, indicating that the range of temperature gradients in these tests is sufficiently large to yield a $CCC_{base} = 0.141$ W K^{-1} value with high confidence. Minor trends are visible in the data, firstly that the CCC is reduced for the experiments in which the ambient temperature is higher. Secondly that the CCC is decreasing as the SOC of the cell reduces. A possible explanation for this, is that the saturation and thickness of the electrodes is affecting the effective thermal conductivity and/or the heat generation profile of the cell [5].

The LG M50T does not appear to show any significant relationships with any of the three variables (I, T & SOC). However, further work would be needed to prove this is the case for more extreme conditions. Similarly, cells other than the LG M50T would need to be similarly checked, as different compositions of electrodes and electrolyte may cause a stronger variation of CCC with these variables.

4.1.2. LG M50T CCC_{Base}

Fig. 5 shows all data gathered for LG M50T cells 1 and 2, with a line of best fit for the full dataset. The CCC_{Base} for the LG M50T is 0.139 W K^{-1} ± 2.8 %, where the error margin is calculated based on the 95 % confidence bounds of the fit, to account for the spread.

The heat flow in the identified loss paths is calculated using the estimated thermal resistance of the individual loss paths and the thermal difference recorded by the TCs. The percentage of heat flowing through the loss path compared to the heat flowing though the fin was calculated as 1.5 % loss from the positive end, including losses through the tab and insulation; and 1.5 % gain at the negative end, through the tab. This indicates that 1.5 % of the heat measured through the fin is not generated by the cell, instead originating in the negative clamps and tab, before conducting into the cell. The proportion is low and has minimal effect on the measured CCC which as such can be assumed accurate.

4.1.3. Pouch cells

A comparison between the CCC values for cylindrical cells and those for pouch cells is meaningful, but not straightforward. CCC for base cooled cylindrical cells is most similar in concept to single tab cooling for pouch cells (that have tabs at either end). Previous CCC work has measured CCC values for dual tab cooling of pouch cells, one of these cells is the Kokam 5 Ah (SLPB11543140H5) [8]. This Kokam cell is comparable to the LG M50T, with similar NMC chemistry and capacity. The Kokam cell has dimensions of 142.5 × 43 × 11.7 mm (L × W × T), with tabs at either end of its length. Under dual tab cooling, the steady state thermal profile of the cell was found to be approximately uniform across the cell's width and thickness, as confirmed via experimental measurements from surface thermocouples and via the output of an electro-thermal model. A thermal gradient was found to develop along the length of the cell. The CCC was defined by the heat flow out of both tabs, divided by the thermal difference from the tabs to the centre of the cell (measured at the surface). Under single tab cooling it is expected that the thermal difference should approximately double for the same heat flow, with a single tab needing to extract heat from the entire length of the cell instead of just half. The thermal difference would be expected to be from one tab to the other, doubling the characteristic length. It is important to note that this is a rough approximation due to many interconnected phenomena affecting the heat flow and generation. However, in terms of order of magnitude estimation, the CCC value for dual tab cooling will be halved and used for comparison. This Kokam cell has a dual-tab cooling CCC of 0.332 W K^{-1} [8], a single tab cooling CCC for this cell would be approximated to be 0.150 W K^{-1}. This value is only 8 % higher, and thus marginally better, than the cylindrical LG M50T cell. Based on these numbers, a reasonable assumption may be that the two cells are thermally similar. However, the characteristic length of the cell impacts the value of the CCC considerably, thus making it an essential property for understanding any comparison between cells with different form factors. The Kokam cell's characteristic length is 150 % greater than that of the LG M50T (113 mm for the Kokam cell, discounting the tabs, versus 70 mm for the LG M50T), thus one might expect the Kokam cell should have a lower CCC than the LG M50T. The similar CCC values for the two cells suggest that the structure of the

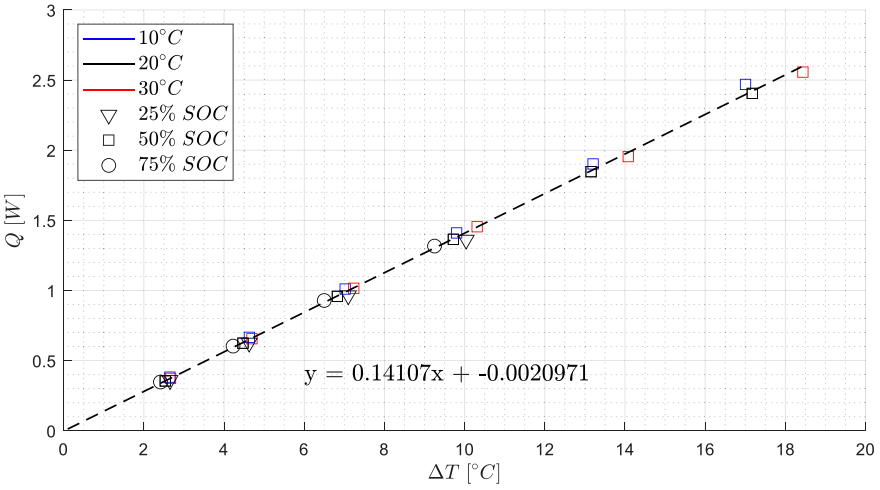

Fig. 4. Measured heat generation versus measured temperature gradient for the LG M50T cell under base cooling, exhibiting a strong linear correlation that enables the calculation of $CCC_{base} = 0.141$ W K^{-1} with high confidence. The symbols correspond to each of the 26 pulsing sets, at six current amplitudes (between 3.75 A and 10 A), three SOCs (between 25 % and 75 %), and three cooling (and ambient) temperatures (between 10 °C and 30 °C).

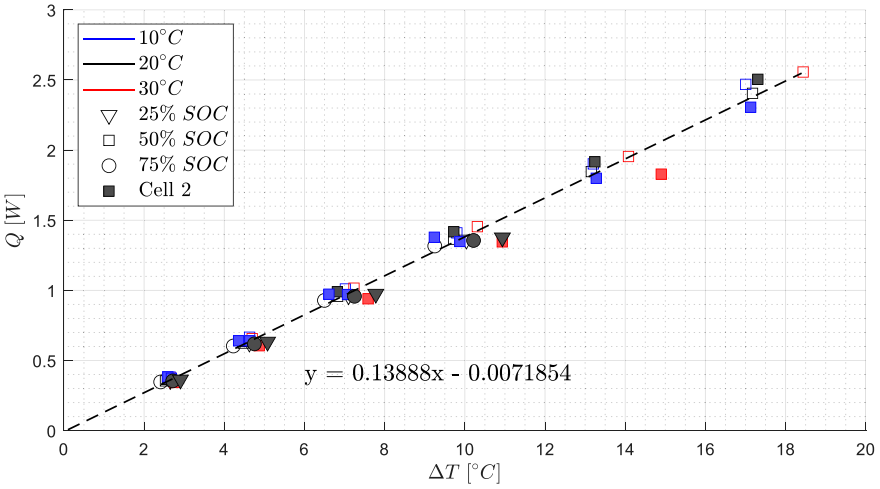

Fig. 5. Measured heat generation versus measured temperature gradient for the LG M50T cell under base cooling, giving a CCC of 0.139 W K^{-1}. The symbols and colours correspond to each of the 51 pulsing sets, at six current amplitudes (between 3.75 A and 10 A), three SOCs (between 25 % and 75 %), three cooling (and ambient) temperatures (between 10 °C and 30 °C), and two LG M50T cells.

Kokam cell is more efficient for tab heat rejection, compared to the structure of the LG M50T for rejecting heat through its base.

4.2. 18650 comparison

The choice between pouch or cylindrical cells will often be based upon several other more influential factors (e.g., configuration, safety, energy/power densities, pack construction). However, the decision between different cylindrical cells, in their various capacities and sizes, may be significantly less rigid and could come down to factors like thermal performance. As part of this work, another popular cylindrical cell form factor is tested, the 18650. Fig. 6 shows the CCC plot for a set of CCC_{Base} data gathered for a 3 Ah Samsung INR18650-30Q cell, under six different currents, ranging from 1C to 3.5C, and three ambient temperatures, 10, 15 and 20 °C. All results are gathered from a single cell at 50 % SOC, with the 20 °C repeat data simply a repeated test of the same cell, where the cell was removed from the rig and subsequently inserted back in. The same nickel tabs and connection position as for the 21700 cell are used, with the cell tested in the same experimental rig. Given that the setup is identical to that in Fig. 3, losses are expected to be of a similar magnitude to the M50T tests, and thus assumed to have minimal effect on the calculated CCC.

The data points lie on a line of fit with small scatter, showing that the data is consistent. The y-intercept is relatively low, indicating a sufficient thermal range for the results to be trustworthy. This line gives a CCC_{Base} of 0.115 W K^{-1} ± 1.5 % for the Samsung 30Q. The two measures of a successful CCC test – the spread of data across a linear fit and the low y-intercept – indicate that this dataset is significantly more consistent than the results from the LGM50; no dependence on ambient temperature and no apparent change in data with a repeat are visible. It could be assumed that the lack of dependency of this data could translate to a consistent and horizontal dataset on the original plot for the CCC (CCC vs. Q) [8].

Fig. 7 shows the same data plotted using the old style representation from Hales et al. [8] It is clear that the data does not sit on a single horizontal line on this plot, each set of six currents has its own heat rejection dependence, with no clear dependence on ambient temperature and a significant effect of a repeat, visible in the two 20 °C tests. The CCC value can only be obtained by calculating the mean of the dataset, yielding a value of 0.120 W K^{-1} ± 6 %. This CCC_{Base} value is about 4 % higher than the value obtained above using the improved method. It is hypothesised that the difference between these two values is a result of

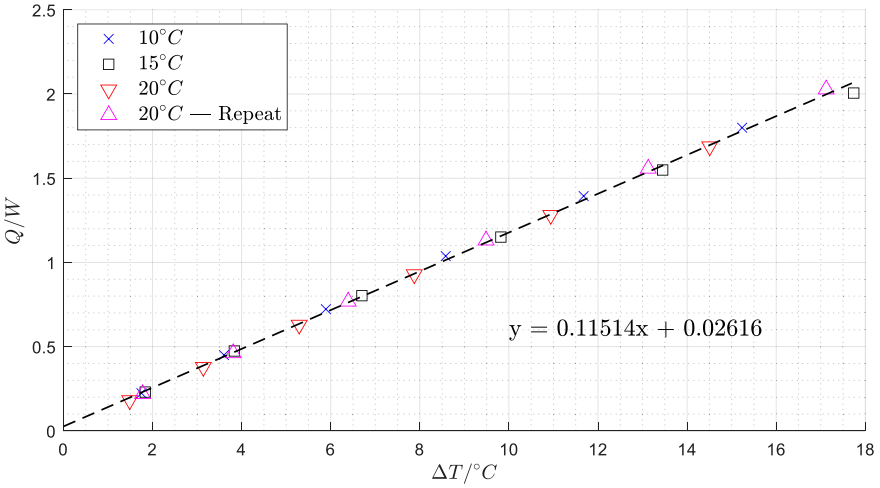

Fig. 6. Measured heat generation versus measured temperature gradient for the Samsung 30Q cell under base cooling, giving a CCC of 0.115 W K^{-1}. The symbols and colours correspond to each of the 24 pulsing sets, at six current amplitudes (between 3 A and 10.5 A, in increments of 1.5 A), three cooling (and ambient) temperatures (between 10 °C and 20 °C), and one repeated test at 20 °C. All tests were performed at 50 % SOC.

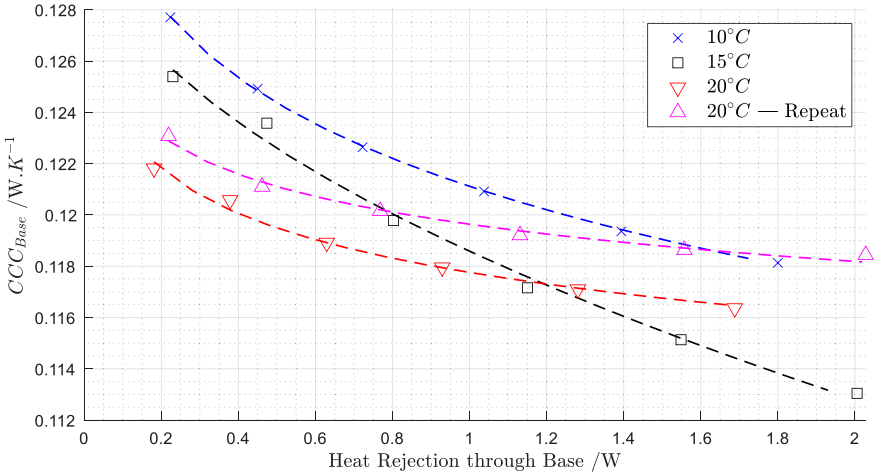

Fig. 7. CCC versus measured heat rejection for the Samsung 30Q. Representing the same data displayed in Fig. 6 using the old CCC representation.

relatively small difference between the absolute temperature of cooling provided by the Peltier element and the temperature of the ambient air in the chamber. This temperature difference results in small steady state heat flows within the rig/cell that affects the measured values of Q and ΔT by a fixed amount. This is hypothesised to affect each individually calculated CCC value shown in Fig. 7, while appearing as a shift in the data on Fig. 6 (the non-zero y-intercept). As a result, the difference in temperatures does not affect the fixed relationship between Q and ΔT (gradient) across multiple values of Q. This indicates that adopting the new CCC plotting procedure helps reduce the uncertainty in determining the CCC value. Fig. 7 leaves room for significant interpretation of the results and how best to determine a singular CCC value, i.e., extrapolate to 0 W, extrapolate to ∞ W, mean of the data, whereas using Fig. 6 removes this, as it simply requires the line of best fit for the data. Additionally, using a line of best fit generates a singular CCC value that conforms to all of the data, as opposed to generating individual CCC values for each data point and attempting to find a singular answer.

4.2.1. 18650 vs 21700 comparison

Comparing the 18650 to the 21700 cell only based on their CCC value is not an accurate representation of their thermal performance in a pack. The 18650 cell is found to have a CCC_{Base} value 16 % lower than that of the 21700 cell, meaning that it can transfer 16 % less heat when at the same temperature difference. However, the 18650 has a base area 36 % smaller than the 21700 through which heat can be transferred during base cooling. Thus, it may be useful to compare heat flux as opposed to total heat flow out of the base of the cells. The ratio CCC/area (CCC") is proposed as an additional tool in this comparison, using the heat flux divided by the temperature difference, as shown in Eq. (2).

$$CCC'' = \frac{CCC}{Area} = \frac{\dot{Q}}{Area}\Big/\Delta T = \dot{Q}''\Big/\Delta T \tag{2}$$

This metric has units of W K^{-1} m^{-2}, identical to the surface heat transfer coefficient (h). However, these two metrics are fundamentally different as h defines the heat flux between two bodies across a 2-D surface for a given temperature difference between the two bodies, whereas the CCC" defines the possible heat flux (of internally generated heat) from a 3-D body through selected 2-D surfaces for a given temperature difference across the 3-D body. The value of the CCC" for the two cells tested is shown in Table 2.

According to this new criterion, the value of the CCC", the 18650 is superior to the 21700. These values predict that, when using multiple cells, as is the case in a pack, the 18650 cells can reject 13 % more heat than the 21700 cells for the same temperature gradient across the cell and the same cooling area of the thermal management system. While the geometry plays a role in this outcome, differences in the internal structure of the two cells are also expected to affect it. This particular 18650 cell is known to have two internal negative tabs, while the 21700 has only one; there may also be differences in electrode and current collector thicknesses, which is expected from the cells having different power/energy densities, as well as the different electrode chemistries (NMC for the 21700 and NCA for the 18650).

Table 2
CCC_{Base}, CCC"$_{Base}$ and $CCC_{GN,Base}$ comparison of 21700 and 18650 cells.

Cell	CCC_{Base} [W K^{-1}]	Base area [m^2]	CCC"$_{Base}$ [W m^{-2} K^{-1}]	Length/area [m^{-1}]	CCC_{Base}*Length/area ($CCC_{GN,Base}$) [W m^{-1} K^{-1}]
21700	0.139	3.46×10^{-4}	401	202	28.1
18650	0.115	2.54×10^{-4}	452	256	29.4

4.2.1.1. Influence of internal composition and structure.

The effect of these internal differences can be accounted for by calculating a CCC normalised for geometry:

$$CCC_{GN} = \frac{\dot{Q}/A}{\Delta T/l} = CCC \times \frac{l}{A}$$

where $\dot{Q}$ is the heat transferred through the cooled surface, $\Delta T/l$ is the temperature gradient from the hottest point to the cooled surface, withΔT being the difference in temperature and l being the distance between these two points, and A is the cross-sectional area of the cooled surface. CCC_{GN} has units of W/m K, identical to thermal conductivity (k). However, k defines the heat flux flowing through a 1-D body for a given temperature gradient (K/m) across the length of the body, whereas CCC_{GN} defines the heat flux of internally generated heat rejected from a 1-D body for a given temperature gradient across the length of the body. Comparing the values of CCC_{GN}, the 18650 is only 5 % better than the 21700. This value predicts that, were the two cells of the same size, there would only be a 5 % difference in CCC between them. Any further differences can be assumed to be the result of the cells' geometry.

4.2.1.2. Geometrical influence.

An estimate of what the CCC for an 18650 with the same internal components and structure as the LG M50T 21700 can be calculated by taking the CCC_{GN} for the 21700 and

multiplying it by the area/length for an 18650. A CCC of 0.110 W K^{-1} is obtained for an 18650 sized LG M50T, a value 21 % lower than that of the CCC for the real 21700 sized LG M50T. When the CCC is normalised to the cooling area of the cells, a value of 432 W/m^2 K indicates a 7 % better CCC" for an 18650 sized LG M50T versus the 21700 sized LG M50T. This analysis is strictly valid only if the value of CCC_{GN} is independent of cell size. These numbers suggest that the CCC favours the 21700 geometry, and the CCC" favours the 18650. This would mean that in a battery pack, a group of 18650 cells are easier to cool (because they are shorter) compared to a group of 21700. However, per cell, each 21700 would be able to reject more heat (because they have a better base area to height ratio) than each 18650.

4.2.1.3. Heat generation. The thermal performance of these cells cannot be compared without considering their heat generation. The heat generation of a lithium-ion cell, however, depends on multiple factors. A recent study demonstrates how extensive testing can help create heat generation maps across multiple conditions, that can be used in conjunction with the CCC to aid cell selection [20]. However, for the purpose of simply comparing heat generation in the two cells, a single set of conditions was chosen; the heat generation was estimated at 1 Hz from the CCC experiments, at 50 % SOC and 20 °C. Even though at this frequency not all the heat generated will be ohmic, an estimate for heat generation can be found by using the overpotentials from the voltage data (V=IR) during the pulsed CCC experiments, estimating heat generation through Joule heating ($Q = I^2R$). The effective R value can be used to estimate heat generation at different currents. The effective internal resistance values extracted are 20 mΩ and 25 mΩ, for the 18650 and the 21700 cell respectively. According to these values, the following predictions can be made:

Under Equal C-Rate – [$Q = C^2R$ (21700: C = 5 A, 18650: C = 3 A), $\Delta T = Q/CCC$]

- The 21700 cell would produce 250 % more heat
- The 21700 cell would have a 180 % larger temperature difference along its length

Under Equal Current – [$Q = I^2R$ (I = 5 A), $\Delta T = Q/CCC$]

- The 21700 cell would generate 25 % more heat.
- The 21700 cell would have a 3 % larger temperature difference along its length

Both comparisons indicate that this 18650 is thermally superior in all scenarios, because the 21700 cell is 25 % more resistive than the 18650 cell according to the measured 1 Hz resistance. However, the CCC of the 18650 cell is only 21 % better than that of the larger cell. In a battery pack, the 21700 compensates for its poorer thermal behaviour by its higher energy density.

The CCC value of a cell has been demonstrated to be a key piece of thermal information [10], despite currently missing from data sheets. The raw CCC indicated that the 21700 is superior, however much of its advantage was found to be the result of geometry, namely its larger base area. Once heat generation is accounted for, the 18650 considered in this study becomes the better cell, in terms of its capability to reject its own heat through its base. How much heat a cell will generate under realistic conditions is also almost impossible to work out from a typical cell data sheet, although there is normally a 1 kHz AC resistance value which can be used for simple calculations, like those above. The above analysis highlights the importance of accounting for factors such as cell geometry, heat generation and capacity when making comparisons between different cells.

5. Conclusions

This work presents a new way to calculate and display the CCC. Heat flow is plotted against the temperature difference measured across the cell, to display a linear relationship where the gradient of the line of best fit is CCC of the cell. The new method simplifies significantly the calculation of CCC for both pouch and cylindrical cells, decreasing the uncertainty in the determined CCC values compared to the previous method [9]. It is shown that CCC experiments must cover the complete thermal range of the cell being tested, to help ensure useful and accurate measurements are made.

A successful experimental rig for determining the CCC of base cooling for cylindrical cells is proposed. A tab welded connection is used at both the positive cap and negative base of the cell. Although not the industry standard for base cooling, this type of connection allows optimal performance of the cell under base cooling, due to negative terminal heat generation being at the closest position to cooling rather than the furthest away (when connected at the shoulder), giving a theoretical maximum CCC_{Base} for the cell. The proposed CCC procedure for the CCC_{Base} of a 21700 cell gives consistent results across multiple currents, SoCs and ambient conditions. This consistency indicates that a single value of CCC_{Base} per cell is required to describe its thermal performance.

Finally, this work displays how the CCC provides a valuable thermal information that, combined with additional metrics, enables the thermal comparison of different cells for down selection during pack design. The CCC_{Base} of the 18650 cell tested is 16 % lower than that of the larger 21700 cell, indicating that the latter is superior. However, when dividing the CCC_{Base} by the cooled area of the bases, the 18650 cell is found to reject 13 % more total heat for the same size cooling area. Furthermore, the 18650 cell would also generate less heat for the same C rate, as it's resistance at 1 Hz was 20 % lower. The 21700 would therefore generate 250 % more heat and have a 180 % larger thermal gradient along its length for an equal C rate. The comparison between form factors is not fair, as the 18650 was a hybrid cell and the 21700 was an energy cell. Instead, it demonstrates the equal importance of understanding heat generation alongside the CCC when designing a cell or down selecting a cell for a particular application. The CCC provides valuable information that is currently missing from cell datasheets, in terms of the cell's thermal dissipation performance.

CRediT authorship contribution statement

M. Waseem Marzook: Writing - original draft, Writing - review & editing, Conceptualisation, Methodology, Investigation, Data curation, Formal Analysis, Visualisation. **Alastair Hales:** Writing - review & editing, Conceptualisation, Methodology, Investigation, Supervision. **Yatish Patel:** Conceptualisation, Methodology, Supervision. **Gregory Offer:** Writing - review & editing, Supervision, Project Administration, Funding Acquisition. **Monica Marinescu:** Writing - review & editing, Supervision, Project Administration, Funding Acquisition.

Declaration of competing interest

The authors declare that they have no known competing financial interests or personal relationships that could have appeared to influence the work reported in this paper.

Data availability

The data presented in this work has been made available at the Zenodo Database and can be accessed through the following DOI: 10.5281/zenodo.6421061.

Acknowledgements

This work was generously supported via an EPSRC CASE (grant number EP/R513052/1) award by Williams Advanced Engineering, as well as the Faraday Institution (grant number EP/S003053/1, FIRG003 & FIRG025), the Innovate UK THT project (grant number 105297), the Innovate UK BATMAN project (grant number 491 104180) and the Innovate UK CoRuBa project (133369).

For the purpose of open access, the author(s) has applied a creative commons attribution (CC BY) licence (where permitted by UKRI, 'open government licence' or 'creative commons attribution no-derivatives (CC BY-ND) licence' may be stated instead) to any author accepted manuscript version arising.

Appendix A. Supplementary data

Supplementary data to this article can be found online at https://doi.org/10.1016/j.est.2022.105217.

References

[1] M. Woody, M. Arbabzadeh, G.M. Lewis, G.A. Keoleian, A. Stefanopoulou, Strategies to limit degradation and maximize Li-ion battery service lifetime - critical review and guidance for stakeholders, J Energy Storage 2020 (28) (October 2019), 101231, https://doi.org/10.1016/j.est.2020.101231.

[2] Z. Tang, A. Song, S. Wang, J. Cheng, C. Tao, Numerical analysis of heat transfer mechanism of thermal runaway propagation for cylindrical lithium-ion cells in battery module, Energies 13 (4) (2020), https://doi.org/10.3390/en13041010.

[3] Y.A. Cengel, A.J. Ghajar, Heat and Mass Transfer, 5th ed., 2015.

[4] S.J. Drake, D.A. Wetz, J.K. Ostanek, S.P. Miller, J.M. Heinzel, A. Jain, Measurement of anisotropic thermophysical properties of cylindrical Li-ion cells, J Power Sources 252 (2014) 298–304, https://doi.org/10.1016/j.jpowsour.2013.11.107.

[5] H. Maleki, Hallaj S. Al, J.R. Selman, R.B. Dinwiddie, H. Wang, Thermal properties of lithium-ion battery and components, J Electrochem Soc. 146 (3) (1999) 947–954, https://doi.org/10.1149/1.1391704.

[6] S.J. Bazinski, X. Wang, Experimental study on the influence of temperature and state-of-charge on the thermophysical properties of an LFP pouch cell, J Power Sources 293 (2015) 283–291, https://doi.org/10.1016/j.jpowsour.2015.05.084.

[7] B. Shi, H. Zhang, Y. Qi, L. Yang, Calculation model of effective thermal conductivity of a spiral-wound lithium ion battery, J. Therm. Sci. 27 (6) (2018) 572–579, https://doi.org/10.1007/s11630-018-1060-x.

[8] A. Hales, L.B. Diaz, M.W. Marzook, Y. Zhao, Y. Patel, G. Offer, The cell cooling coefficient: a standard to define heat rejection from lithium-ion batteries, J. Electrochem. Soc. 166 (12) (2019) A2383–A2395, https://doi.org/10.1149/2.0191912jes.

[9] A. Hales, M.W. Marzook, L. Bravo Diaz, Y. Patel, G. Offer, The surface cell cooling coefficient: a standard to define heat rejection from lithium ion battery pouch cells, J. Electrochem. Soc. 167 (2) (2020), 020524, https://doi.org/10.1149/1945-7111/ab6985.

[10] A. Hales, R. Prosser, L. Bravo Diaz, G. White, Y. Patel, G. Offer, The cell cooling coefficient as a design tool to optimise thermal management of lithium-ion cells in battery packs, eTransportation 6 (2020), 100089, https://doi.org/10.1016/j.etran.2020.100089.

[11] A.A. Pesaran, G.-H. Kim, K. Smith, E.C. Darcy, Designing safe lithium-ion battery packs using thermal abuse models, NREL. NREL/PR (540–45388) (2008).

[12] X.Y. Yao, L. Kong, M.G. Pecht, Reliability of cylindrical li-ion battery safety vents, IEEE Access. 8 (2020) 101859–101866, https://doi.org/10.1109/ACCESS.2020.2997792.

[13] E. Darcy, F. Davies, J. Jeevarajan, P. Cowles, Lithium-ion cell PTC limitations and solutions for high voltage battery applications, Electrochem. Soc. 203rd Meet. 1 (2003). https://www.electrochem.org/dl/ma/203/pdfs/0189.pdf.

[14] J.B. Robinson, J.A. Darr, D.S. Eastwood, et al., Non-uniform temperature distribution in Li-ion batteries during discharge - a combined thermal imaging, X-ray micro-tomography and electrochemical impedance approach, J Power Sources 252 (2014) 51–57, https://doi.org/10.1016/j.jpowsour.2013.11.059.

[15] C. Bolsinger, K.P. Birke, Effect of different cooling configurations on thermal gradients inside cylindrical battery cells, J. Energy Storage 2019 (21) (September 2018) 222–230, https://doi.org/10.1016/j.est.2018.11.030.

[16] D. Worwood, R. Algoo, R.J. McGlen, J. Marco, D. Greenwood, A study into different cell-level cooling strategies for cylindrical lithium-ion cells in automotive applications, Int. J. Powertrains 7 (1–3) (2018) 199–226, https://doi.org/10.1504/IJPT.2018.090381.

[17] S. Li, N. Kirkaldy, C. Zhang, et al., Optimal cell tab design and cooling strategy for cylindrical lithium-ion batteries, J. Power Sources 492 (February) (2020). https://www.researchgate.net/publication/346728587_Optimal_cell_tab_design_and_cooling_strategy_for_cylindrical_lithium-ion_batteries.

[18] National Physical Laboratory, Thermal performance, NPLWebsite, https://www.npl.co.uk/products-services/advanced-materials/thermal-performance. (Accessed 27 January 2022).

[19] X. Hua, C. Heckel, N. Modrow, et al., The prismatic surface cell cooling coefficient: a novel cell design optimisation tool & thermal parameterization method for a 3D discretised electro-thermal equivalent-circuit model, eTransportation 7 (2021), 100099, https://doi.org/10.1016/j.etran.2020.100099.

[20] L. Bravo Diaz, A. Hales, M.W.J. Marzook, Y. Patel, G.J. Offer, Measuring irreversible heat generation in lithium-ion batteries: an experimental methodology, J. Electrochem. Soc. (2022), https://doi.org/10.1149/1945-7111/ac5ada.

[21] G. White, A. Hales, Y. Patel, G. Offer, Novel methods for measuring the thermal diffusivity and the thermal conductivity of a lithium-ion battery, Appl. Thermal Eng. 212 (2022), https://doi.org/10.1016/j.applthermaleng.2022.118573.